ZnO Clusters Encapsulated inside Micropores of Zeolites Studied by UV Raman and Laser-Induced Luminescence Spectroscopies

Jun Chen, Zhaochi Feng, Pinliang Ying, and Can Li*

State Key Laboratory of Catalysis, Dalian Institute of Chemical Physics, Chinese Academy of Sciences, P.O. Box 110, Dalian 116023, China

Received: March 22, 2004; In Final Form: June 9, 2004

Using microporous zeolites as host, sub-nanometric ZnO clusters were prepared in the micropores of the host by the incipient wetness impregnation method. A small amount of sub-nanometric ZnO clusters were introduced into the channels of HZSM-5 zeolite, whereas a large quantity of sub-nanometric ZnO clusters can be accommodated in the supercages of HY zeolite and no macrocrystalline ZnO exists on the extra surface of the HY material. The vibrations of the zeolite framework and ZnO were characterized by UV Raman spectroscopy. The optical properties of these ZnO clusters were studied by UV−visible absorption spectroscopy and laser-induced luminescence spectroscopy. It is found that there are strong host−guest interactions between the framework oxygen atoms of zeolite and ZnO clusters influencing the motions of the framework oxygen atoms. The interaction may be the reason why ZnO clusters are stabilized in the pores of zeolites. Different from bulk ZnO materials, these sub-nanometric ZnO clusters exhibit their absorption onset below 265 nm and show a purple luminescence band (centered at 410−445 nm) that possesses high quantum efficiency and quantum size effect. This purple luminescence band most likely originates from the coordinatively unsaturated Zn sites in sub-nanometric ZnO clusters. On the other hand, the differences in the pore structure between HZSM-5 and HY zeolites cause the absorption edge and the purple luminescence band of ZnO clusters in ZnO/HZSM-5 show a red shift in comparison with those of ZnO clusters in ZnO/HY.

Introduction

In recent years, semiconductor ZnO has attracted much attention due to its promising applications in commercial devices such as a high-efficiency low-voltage phosphor, UV-light emitter, and for solar cells, and therefore the unique optical properties of ZnO have been exploited.[1−3] As we know, when the particle sizes of many semiconductors, ZnO included, decrease to nanometer or sub-nanometer scales, these materials usually exhibit quantum size effects, presenting different electric and optical properties from bulk materials.[4−6] The study on sub-nanometric ZnO clusters as a medium between single molecules and nanocrystals is an active area now days,[7−11] but their luminescent properties are rarely reported. Since ZnO clusters are so small and unstable, many materials, such as glass, polymers and zeolites, are used as supports or stabilizers in the various preparation methods.[8,12−14] Using microporous zeolites as host, they provide well-defined and well-ordered pores to confine the ZnO clusters. Thus, the size and configuration of ZnO clusters can be tailored using different microporous zeolites. On the other hand, ZnO clusters encapsulated in the zeolites show catalytic activity for some reactions.[15,16]

In this work, different amounts of ZnO clusters were prepared in the pores of HZSM-5 (MFI type) and HY (FAU type) microporous zeolites by the incipient wetness impregnation method. The host−guest interactions between the zeolite framework and ZnO clusters were characterized by UV Raman spectroscopy, which greatly enhances the Raman scattering and avoids the interference of fluorescence.[17−21] The optical properties of these ZnO clusters were studied by UV−visible absorption spectroscopy and laser-induced luminescence (LIL) spectroscopy. It is observed that the ZnO clusters exhibit significantly different optical behaviors from bulk ZnO materials, showing a very strong purple luminescence band and evident quantum size effects.

Experimental Section

1. Sample Preparation. ZnO clusters encapsulated inside zeolites were prepared by the incipient wetness impregnation method. Two types of microporous zeolites, HZSM-5 and HY, were used as the host materials, respectively. HZSM-5 was obtained by calcining NH_4ZSM-5 (CBV 8014, Zeolyst International, $SiO_2/Al_2O_3 = 80$) at 550 °C for 5 h. HY (CBV 720, Zeolyst International, $SiO_2/Al_2O_3 = 30$) was also calcined at 550 °C for 5 h. Then, they are sealed and put in the desiccator to protect against the adsorption of water. A special volume (the maximum adsorption volume for 1.00 g of zeolite power) of $Zn(NO_3)_2$ aqueous solution was added into 1.00 g of zeolite powder with continuous stirring. This mixture was held for 1 h, and then it was stirred under a hot water bath until dried. After this powder was kept at 120 °C overnight, it was calcined at 550 °C for 5 h. Thus, ZnO/HZSM-5 and ZnO/HY materials were obtained. To achieve different ZnO loadings materials, the concentration of $Zn(NO_3)_2$ aqueous solution was adjusted. The preparation process and conditions of ZnO/SiO_2 with 1.0 wt % ZnO loading, using SiO_2 powder as substrate, were the same as that of ZnO/HZSM-5 and ZnO/HY.

2. Spectroscopy Measurement. UV Raman spectra were collected by a home-built UV Raman spectrograph.[17−21] The luminescence measurements were performed using a home-built laser-induced luminescence spectroscopy setup. The lumines-

* To whom correspondence should be addressed. Fax: +86−411−84694447. Tel: +86−411−84379070. E-mail: canli@dicp.ac.cn. Home page: http://www.canli.dicp.ac.cn.

10.1021/jp048746x CCC: $27.50
Published on Web 08/04/2004

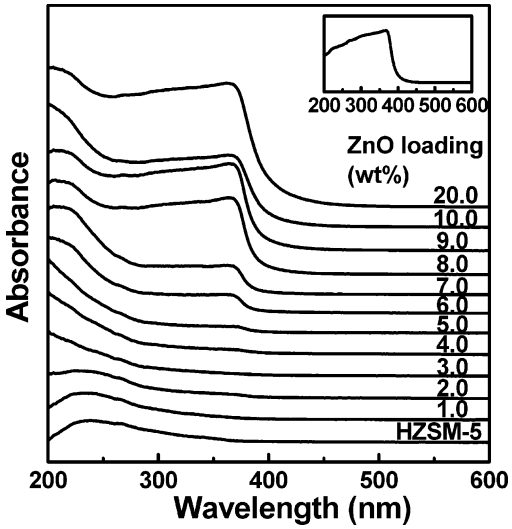

Figure 1. UV−visible absorption spectra of ZnO/HZSM-5 with different ZnO loadings. The spectrum of HZSM-5 was added for comparison. The inset shows the UV−visible absorption spectrum of ZnO/SiO_2 with 1.0 wt % ZnO loading.

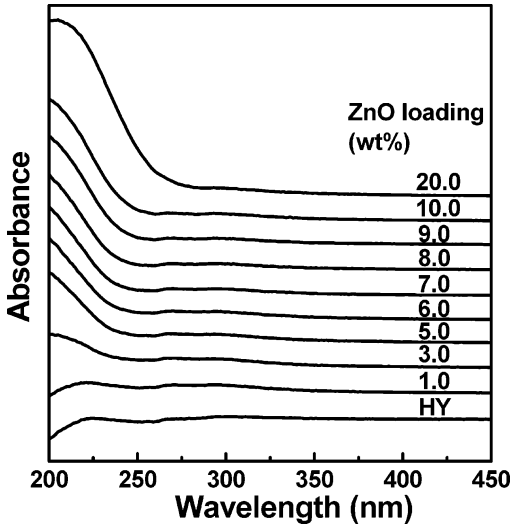

Figure 2. UV−visible absorption spectra of ZnO/HY with different ZnO loadings. The spectrum of HY was added for comparison.

cence output was collected with an ellipsoidal collecting mirror and focused onto a 32 cm monochromator (Jobin-Yvon Triax 320) by passing through a filter. CCD (Jobin-Yvon Spectrum One CCD 3000) was mounted at the focal plane in the exit of the monochromator to detect the luminescence signal. A computer and the software GRAMS/32 were used to control the monochromator and CCD and to analyze the data. Prior to the experiments, the wavelength calibration of this setup was carried out with a mercury lamp. Two continuous wave lasers, a He−Cd laser ($\lambda = 325$ nm) and a frequency-doubled Ar ion laser ($\lambda = 244$ nm), were used as the excitation sources for UV Raman and LIL spectroscopy. UV−visible absorption spectra were recorded on a JASCO V-550 spectrophotometer equipped with an integrating sphere. All these spectral measurements were carried out in air at room temperature.

3. X-ray Diffraction, Transmission Electron Microscope, and Physisorption Analysis. The powder X-ray diffraction (XRD) patterns were recorded on a Rigaku MiniFlex diffractometer with Cu Kα radiation source. The 2θ range is 5°−75° at a step size of 0.02° and a scanning speed of 8°/min.

Transmission electron microscope (TEM) measurements were taken on a JEOL JEM-2000EX electron microscope with an acceleration voltage of 100 kV.

Adsorption isotherms were recorded in static mode, and N_2 was used as the analysis gas at 77 K. For ZnO/HZSM-5 samples, the BET surface area was obtained on an ASAP 2000 system. For ZnO/HY samples, sorption experiments were performed on a Quantachrome Instruments Autosorb-1, and the density functional theory (DFT) equilibrium model was applied to analyze the pore distribution and the cumulative pore volume.

Results and Discussion

1. ZnO Clusters in Zeolites Characterized by UV−Visible Absorption Spectroscopy, XRD, and TEM. Figure 1 shows the UV−visible absorption spectra of ZnO/HZSM-5 with increasing ZnO loading. After subtracting the optical absorption of host HZSM-5, it is observed that all these ZnO/HZSM-5 exhibit an absorption band with the absorption onset at about 265 nm. Another absorption band at about 370 nm, which corresponds to the band gap width of macrocrytalline ZnO, appears when the ZnO loading exceeds 4.0 wt % and develops obviously with increasing ZnO loading. It is known that if the size of ZnO particle decreases to the order of the Bohr radius, the width of the band gap increases as the particle becomes smaller, and the optical absorption shows a blue shift. It was reported that the absorption onset locates at 265−270 nm, corresponding to a ZnO cluster with a diameter around 10 Å.[22] In addition, Haase et al. gave an empirical curve of absorption onset wavelength vs particle size, showing that the mean size of ZnO clusters at 10 Å corresponds to about 280 nm.[23] The theoretical calculation by Brus predicted that the absorption onset would be much shorter than 280 nm for a ZnO cluster of 10 Å diameter.[24,25] These results indicate that ZnO clusters, having an optical absorption with onset wavelength at about 265 nm, are formed in the pores of HZSM-5 for low ZnO loading. But the high loading leads to the formation of the macrocrystal particle of ZnO on the extra surface of HZSM-5. On the other hand, as shown in the inset of Figure 1, the appearance of the absorption band at 370 nm demonstrates that the macrocrystal particle of ZnO is formed for ZnO/SiO_2, even with 1.0 wt % ZnO loading. This again confirms that ZnO clusters are formed in the pores of HZSM-5 for ZnO/HZSM-5 samples with low ZnO loading.

Figure 2 shows the UV−visible absorption spectra of ZnO/HY with increasing ZnO loading, where the host HY zeolite has the sodalite cage with a diameter of 6.6 Å and the supercage with a diameter of 11.8 Å. All samples exhibit an absorption band with the onset wavelength between 240 and 260 nm, while the absorption onset shows a red shift as the ZnO loading increases. On the other hand, the absorption of macrocrystalline ZnO is not observed, even for ZnO loading as high as 20.0 wt %. This indicates that ZnO clusters have been formed mainly in the pores of HY, where ZnO clusters grow upon increasing the ZnO loading, and no macrocrystalline ZnO exists on the extra surface of HY zeolite.

Figure 3 shows the XRD patterns of ZnO/HZSM-5 with different ZnO loadings. All these materials maintain good zeolite crystal structure. At low ZnO loading, no diffraction peak of macrocrystalline ZnO exists. At high ZnO loading, the diffraction peaks of ZnO with wurtzite structure appear and develop with increasing loading. These results are consistent with those of UV−visible absorption spectroscopy characterization. For the ZnO/HY materials, as shown in Figure 4, all samples with different ZnO loadings not only retain good zeolite crystal structure but also do not exhibit the diffraction peaks of macrocrystalline ZnO. It again demonstrates that ZnO clusters

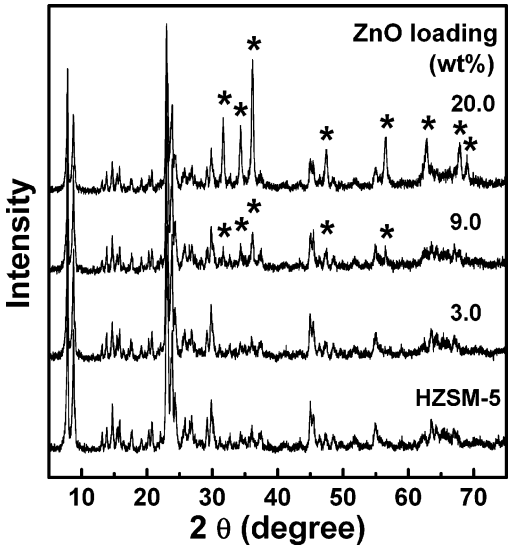

Figure 3. XRD patterns of ZnO/HZSM-5 with different ZnO loadings. The asterisk shows the diffraction peaks of ZnO crystal with wurtzite structure. The XRD pattern of HZSM-5 was added for comparison.

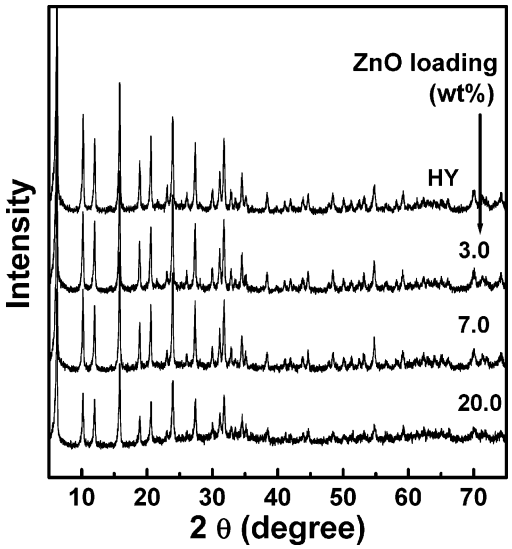

Figure 4. XRD patterns of ZnO/HY with different ZnO loadings. The XRD pattern of HY was added for comparison.

have been formed in the pores of HY and no macrocrystalline ZnO exists. Figure 5 shows the TEM pictures of ZnO/HZSM-5 and ZnO/HY samples with 20.0 wt % ZnO loading. It is clearly observed that some ZnO particles covered the extra surface of HZSM-5, but no image of ZnO particles has been found on the outside surface of HY.

These results suggest that the pore structures of microporous zeolites would influence the amount of ZnO clusters encapsulated inside the pores for ZnO/zeolite prepared by the incipient wetness impregnation method. For the host HZSM-5 zeolite, its narrow, straight channels are unfavorable for the transmission of the zinc precursor, water vapor, and the products from the decomposition of zinc nitrate at high temperature. Thus, only a small amount of ZnO clusters could be introduced into the channels of HZSM-5. For the host HY zeolite, it has a three-dimensional pore system: a supercage connects with four supercages through the twleve-member ring and connects with four sodalite cages through the six-member ring. This pore system is favorable for the transmission of the compounds in the preparation process of ZnO/HY. Thus, a large amount of ZnO clusters can be accommodated in the cages of HY, and no

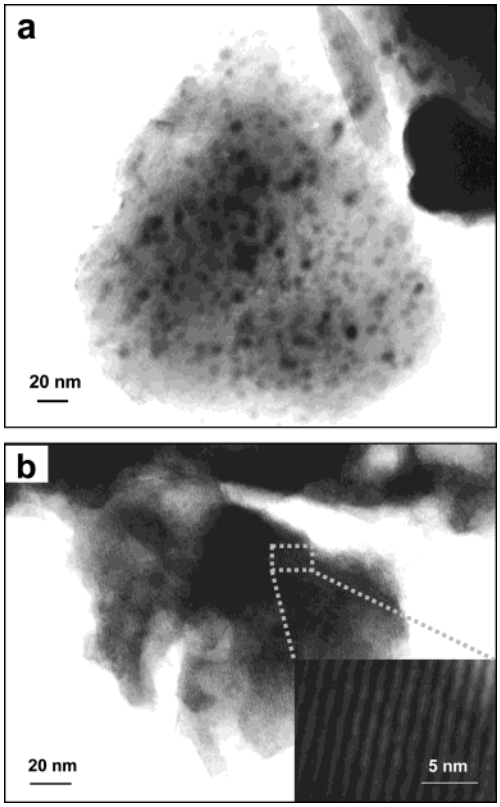

Figure 5. TEM pictures of 20.0 wt % ZnO loading (a) ZnO/HZSM-5 and (b) ZnO/HY samples.

TABLE 1: Physical Properties of ZnO/HZSM-5 and ZnO/HY with Different ZnO Loadings

	ZnO/HZSM-5					
ZnO loading (wt %)	0	1.0	3.0	4.0	7.0	8.0
BET surface area (m^2/g)	394	390	372	370	362	347
	ZnO/HY					
ZnO loading (wt %)	0	5.0	8.0	10.0	20.0	
BET surface area (m^2/g)	771	757	714	677	554	
cumulative pore volume (cm^3/g) for pore diameter < 7.17 Å	0.042	0.039	0.037	0.040	0.042	
cumulative pore volume (cm^3/g) for pore diameter < 21.13 Å	0.320	0.310	0.288	0.278	0.226	

macrocrystalline ZnO is formed outside of the pores. Furthermore, compared with the ZnO clusters formed inside the channels (diameter of ca. 5.5 Å) of HZSM-5, the absorption onset of ZnO clusters in ZnO/HY locates at shorter wavelength, suggesting that the ZnO clusters in ZnO/HY are smaller than those in ZnO/HZSM-5. The reason may be that clubbed ZnO clusters have been formed in the straight channels of HZSM-5, whereas spherical ZnO clusters are confined in the cages of HY.

2. Pore Textures of ZnO/HZSM-5 and ZnO/HY. Zeolites are used as the hosts to confine the ZnO clusters, because they have well-defined and well-ordered pores. The information on the pore texture of ZnO/zeolite will help us to understand the status of ZnO clusters encapsulated in the hosts. Here, the physisorption method was adopted to analyze the texture properties of ZnO/HZSM-5 and ZnO/HY with different ZnO loadings. All the adsorption isotherms of these materials exhibit the type I isotherm as defined by Brunauer,[26] indicating the characteristic of a microporous adsorbent. Table 1 shows the physisorption values of these materials. The BET surface area

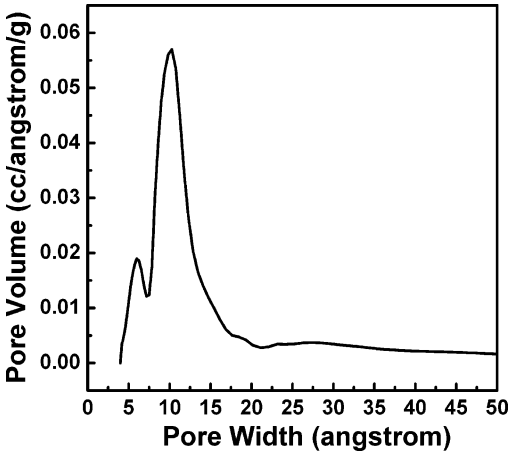

Figure 6. Microporous volume distribution of HY analyzed by DFT method.

of both ZnO/HZSM-5 and ZnO/HY samples decreases with increasing ZnO loading. This suggests that the pores of zeolites are partly occupied by ZnO clusters.

HY zeolite has two kinds of cavities, sodalite cage and supercage. The knowledge of where the clusters locate in HY is very important for estimating the size of the cluster and understanding the interaction between the host framework and the clusters. In this case, DFT method was applied to analyze the pore size distribution and the cumulative pore volume of ZnO/HY samples. Figure 6 shows the micropore size distribution of HY. It exhibits two peaks at 6.0 and 10.3 Å, which are respectively approximate to the pore diameter of the sodalite cage and supercage. In addition, analyzed from this figure, the cumulative pore volume for pores smaller than 7.17 Å is 0.042 cm^3/g and that for pores smaller than 21.13 Å is 0.320 cm^3/g. These two volume values are quite agreeable with the total sodalite cage volume and the total pore volume of HY, respectively. This demonstrates that the DFT method well describes the pore distribution of HY. Table 1 presents the cumulative pore volume of ZnO/HY with different ZnO loadings. It is shown that the cumulative pore volume for pores smaller than 7.17 Å remains mostly unchanged for these ZnO/HY samples, but for pores smaller than 21.13 Å, the cumulative pore volume decreases obviously upon increasing the ZnO loading, meaning that the total volume from sodalite cages remains unchanged and the total volume from supercages decreases as the ZnO loading is increased. These results demonstrate that most ZnO clusters are confined within the supercages, but the ZnO cluster is scarcely formed in the sodalite cage.

3. Interaction between Host Framework and ZnO Clusters Characterized by UV Raman Spectroscopy. Raman spectroscopy is a good technique to provide the bonding and structural information, which is useful for understanding the host−guest interactions between zeolite framework and clusters. But, the visible Raman spectroscopy technique often encounters two problems for characterizing zeolite samples, low Raman scattering cross section and the interference of strong fluorescence background. Thus, to obtain the Raman signal, great efforts must be made to carefully remove the luminescent species, such as a small amount of template agents, from the zeolites. Furthermore, rigorous treatment may destroy the samples. Here, UV Raman spectroscopy was applied to characterization of the ZnO/HZSM-5 and ZnO/HY samples, and no special treatment was performed to avoid the fluorescence interference. This technique, using ultraviolet laser lines as

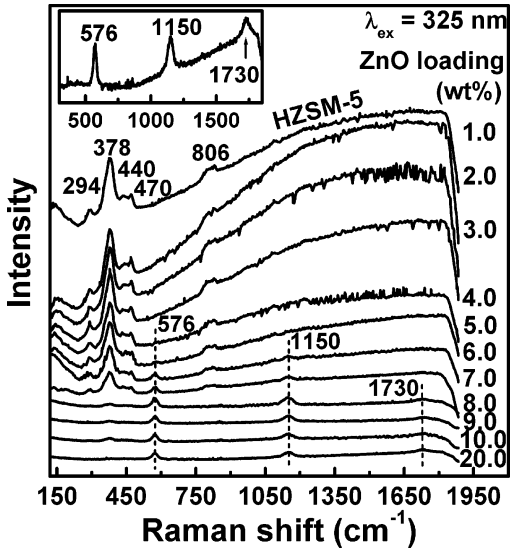

Figure 7. UV Raman spectra of ZnO/HZSM-5 with different ZnO loadings, excited by a 325 nm laser. The inset shows the amplified UV Raman spectrum of ZnO/HZSM-5 with 20.0 wt % ZnO loading.

excitation source, not only enhances the Raman intensity but also successfully avoids the interference of fluorescence, because the Raman spectrum shift from the visible to the ultraviolet region.[17−21,27−29] Two laser lines were respectively used to excite the samples for obtaining the UV Raman spectra; one is 325 nm, which is out of the absorption band of sub-nanometric ZnO clusters but in the absorption band of macrocrystalline ZnO, and another is 244 nm, which is in the absorption band of sub-nanometric ZnO clusters.

Figure 7 shows the UV Raman spectra of ZnO/HZSM-5 with increasing ZnO loading using 325 nm laser as the excitation source. For the samples with ZnO loading below 4.0 wt %, the Raman bands[21] of HZSM-5 at 294, 378, 440, 470, and 806 cm^{-1} keep steady, but the bands between 1090 and 1230 cm^{-1} assigned to nonsymmetric Si−O stretching vibrations[30] cannot be observed, possibly due to fluorescence interference in the high wavenumber region. When the loading exceeds 4.0 wt %, the Raman peaks of HZSM-5 are gradually weakened and eventually disappear with increasing ZnO loading. At the same time, the spectra exhibit the resonant Raman scattering of the ZnO E_{1L} phonon at 576 cm^{-1} and its multiple frequency bands at 1150 and 1730 cm^{-1}. Multiple phonon scattering was previously observed in bulk ZnO crytal materials.[31] These results further indicate that ZnO clusters are formed in the channel of HZSM-5 at low loading, and macrocrystalline ZnO particles are derived on the extra surface of HZSM-5 when ZnO loading is beyond 4.0 wt %. Furthermore, macrocrystalline ZnO particles strongly absorb light shorter than 370 nm, meaning that they not only absorb the 325 nm excitation light but also absorb the Raman signals emitted from HZSM-5. Thus, the Raman bands of HZSM-5 becoming weaker as the loading increases indicates that the amount of macrocrystalline ZnO on the extra surface of HZSM-5 increases with increasing ZnO loading.

Figure 8 shows the UV Raman spectra of ZnO/HZSM-5 with increasing ZnO loading, excited by a 244 nm laser. It is observed that HZSM-5 exhibits Raman bands at 294, 372, 460 (superposition of bands at 440 and 470 cm^{-1}), 806, 1103, 1165, and 1220 cm^{-1}. The Raman bands assigned to nonsymmetric Si−O stretching vibrations at 1103, 1165, and 1220 cm^{-1} appear due to avoiding completely the interference of fluorescence. For ZnO/HZSM-5 samples with different ZnO loadings, the intensity changes of Raman bands belonging to HZSM-5 are the same

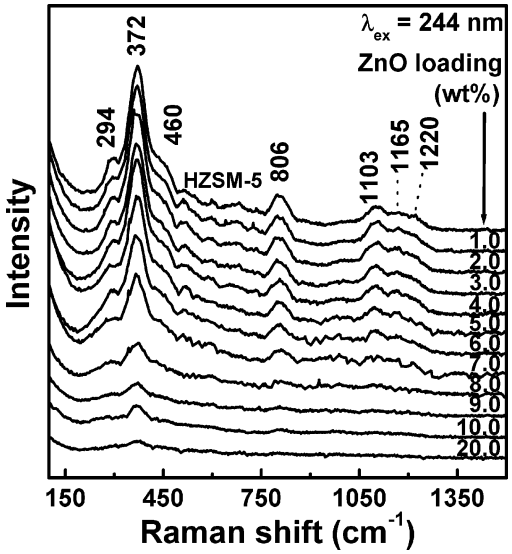

Figure 8. UV Raman spectra of ZnO/HZSM-5 with different ZnO loadings, excited by a 244 nm laser.

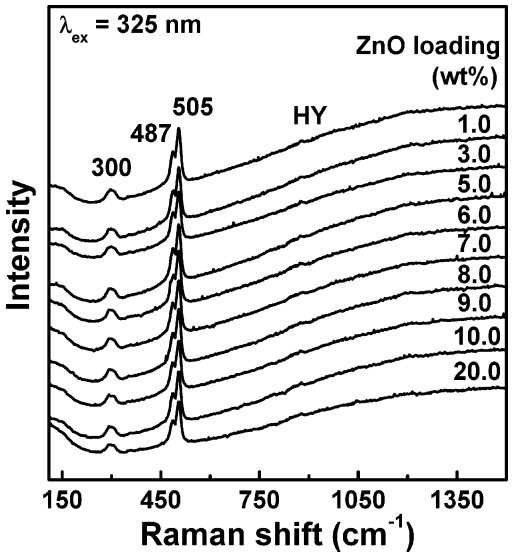

Figure 9. UV Raman spectra of ZnO/HY with different ZnO loadings, excited by a 325 nm laser.

as those spectra excited by 325 nm. This again indicates that ZnO clusters are confined in the channel of HZSM-5 at low loading and that macrocrystalline ZnO particles are formed on the extra surface of HZSM-5 when ZnO loading is beyond 4.0 wt %. But the resonant Raman scattering of macrocrystalline ZnO is not observed for all these samples. The reason may be that the Raman signals are absorbed significantly by surrounding macrocrystalline ZnO species, because the wavelength of the Raman signal excited by 244 nm is much shorter than the absorption edge of the macrocrystalline ZnO. Furthermore, it is difficult to detect the influence of the encapsulated ZnO clusters on the vibrations of the HZSM-5 framework, because the amounts of the ZnO clusters is relatively small and the interference from macrocrystalline ZnO exists.

Figure 9 shows the UV Raman spectra of ZnO/HY with increasing ZnO loading, excited by a 325 nm laser. All the samples just give the Raman bands[21] at 300, 487, and 505 cm^{-1} due to HY. Different from ZnO/HZSM-5, the intensities of these Raman bands remain steady as ZnO loading increases. The Raman bands[32] of HY above 800 cm^{-1} are not observed, possibly due to the fluorescence interference in the high wavenumber region. On the other hand, no resonant Raman

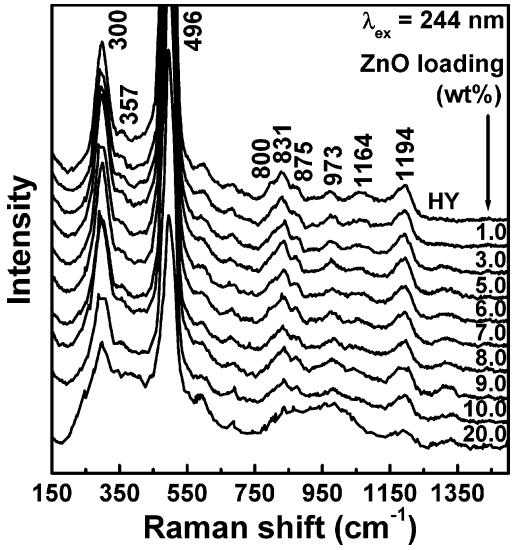

Figure 10. UV Raman spectra of ZnO/HY with different ZnO loadings, excited by a 244 nm laser.

TABLE 2: Assignments of the UV Raman Bands of HY

band position/cm^{-1} (refs)			
T−O−T bending modes			
six-membered rings	four-membered rings	motion of Si atom in tetrahedral cage	Si−O stretching vibration
300, 357 (32, 33)	487, 505 (32, 34, 35)	800, 831, 875 (32)	973, 1164, 1194 (32, 35, 36)

bands of macrocrystalline ZnO are detected for all these samples, in contrast to ZnO/HZSM-5. These results demonstrate that most ZnO have been formed as sub-nanometric ZnO clusters within the pores of HY, even for ZnO loading as high as 20.0 wt %, and no macrocrystalline ZnO particles exist. This is consistent with the conclusions from the characterizations of UV−visible absorption spectroscopy, XRD, and TEM. Besides, no significant absorption of 325 nm light and Raman signals by these ZnO clusters exists, as shown in Figure 2; this is why the Raman scattering of HY is hardly influenced by the ZnO clusters, even for high loading ZnO/HY samples.

Figure 10 shows the UV Raman spectra of ZnO/HY with increasing ZnO loading, excited by a 244 nm laser. The Raman bands of HY appear at 300, 357, 496 (superposition of 487 and 505 cm^{-1} shown in Figure 9), 800, 831, 875, 973, 1164, and 1194 cm^{-1}. As ZnO loading increases to 9.0 wt % for ZnO/HY samples, Raman bands at 300, 496, 800, 831, 875, and 1194 cm^{-1} remain mostly unchanged; the band at 973 cm^{-1} becomes stronger and broader, while the intensity of the band at 1164 cm^{-1} decreases. Upon further increasing ZnO loading, the intensities of the bands at 300, 496, 800, 831, 875, and 1194 cm^{-1} are reduced; also, enhancement and widen continue for the band at 973 cm^{-1}, and the band at 1164 cm^{-1} is further weakened.

Table 2 gives the assignments of the observed vibration bands of zeolite HY in Figure 10. In the region 900−1250 cm^{-1}, several Raman bands are assigned to Si−O stretches of different types of framework oxygen atoms and are localized on the motions of oxygen atoms.[32,35−38] In our case, three bands are observed in this region. As the ZnO loading increases, the intensity of the band at 973 cm^{-1} increases and that at 1164 cm^{-1} decreases. This indicates that there are interactions between the framework oxygen atoms and the ZnO clusters encapsulated inside the pores of HY, influencing the motions of the framework oxygen atoms. When the amount of ZnO

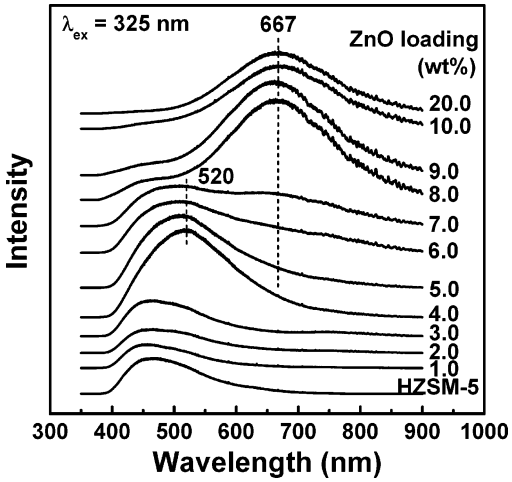

Figure 11. Laser-induced luminescence spectra of ZnO/HZSM-5 with different ZnO loadings, excited at 325 nm.

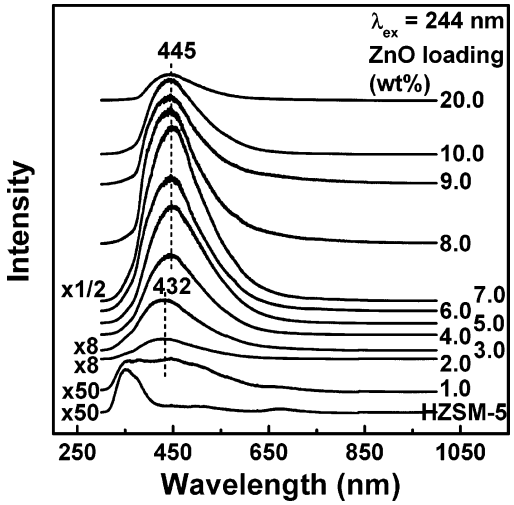

Figure 12. Laser-induced luminescence spectra of ZnO/HZSM-5 with different ZnO loadings, excited at 244 nm.

clusters confined in the supercages of HY is large, such as the ZnO/HY with 20.0 wt % loading (corresponding to an average of 6 ZnO molecules per supercage), the interactions between the framework oxygen atoms of HY and ZnO clusters are evident, as shown in Figure 10. In general, the sub-nanometric cluster is very unstable, because a large quantity of coordinatively unsaturated sites exist in the outer layer.[39,40] The requirement to saturate these coordinatively unsaturated sites provides a tremendous driving force for stabilizing the sub-nanometric ZnO clusters in zeolite channels or cavities. In the case of ZnO/HY materials, the coordinatively unsaturated zinc sites of the ZnO cluster encapsulated inside the supercage strongly interact with the framework oxygen atoms. This is most likely the reason why a large amount of ZnO clusters can be stabilized inside the pores of HY zeolite.

4. Luminescence Characteristics of ZnO/HZSM-5 and ZnO/HY. To follow UV Raman characterization, two laser lines at 244 and 325 nm were selected as excitation sources to study the luminescence characteristics of these materials. Figure 11 shows the LIL spectra of ZnO/HZSM-5, excited at 325 nm. The samples with ZnO loading below 4.0 wt % exhibit a broad luminescence band centered at 460 nm, which is the same as that of HZSM-5.When the ZnO loading is increased to 4.0 wt %, the sample obviously shows a green luminescence band centered at 520 nm. Upon further increasing the loading, this green band is gradually weakened, while an orange luminescence band centered at 667 nm emerges and becomes stronger. The appearance of the orange band suggests that macrocrystalline ZnO is formed for the samples with high ZnO loading. This is consistent with the conclusions from UV−visible absorption spectra and UV Raman spectra. From our previous studies, it is realized that the green band originates from the high density of oxygen vacancies in ZnO, and the orange band is ascribed to the state with less oxygen vacancies. For the samples with loading between 4.0 and 7.0 wt %, a little amount of small ZnO particles are formed on the extra surface of HZSM-5. These ZnO particles, with a high density of oxygen vacancies due to their large ratio of surface area to volume, exhibit a green luminescence band. With an increasing loading, ZnO crystals covering on the extra surface of HZSM-5 grow up, and the density of oxygen vacancies decreases. Thus, the samples with high ZnO loading show the orange luminescence band.

Figure 12 shows the LIL spectra of ZnO/HZSM-5 with increasing ZnO loading, excited at 244 nm. All ZnO/HZSM-5 samples exhibit a purple luminescence band centered at about 440 nm. The intensity of this band increases significantly with increasing ZnO loading up to 7.0 wt %, while the peak position shifts from 432 to 445 nm. Upon further increasing ZnO loading, this band becomes weaker. On the other hand, from this figure we cannot see the green luminescence band (centered at 520 nm) or the orange luminescence band (centered at 667 nm) shown in Figure 11, whereas this purple luminescence band cannot be observed in Figure 11. From the UV−visible absorption spectra, it is clearly shown that the excitation wavelength of 244 nm locates in the absorption band of the ZnO clusters in ZnO/HZSM-5, whereas the excitation wavelength of 325 nm is out of the absorption band of ZnO clusters but inside the absorption region of macrocrystalline ZnO. This means that 325 nm light cannot excite the electron of the ZnO clusters in ZnO/HZSM-5 from the ground state to the upper electronic state, whereas 244 nm light can. These results demonstrate that the purple luminescence band centered at about 445 nm arises from the sub-nanometric ZnO clusters encapsulated in HZSM-5. Furthermore, the development of the amount of macrocrystalline ZnO, which strongly absorbs 244 nm light, covering the extra surface of HZSM-5 will reduce the light irradiation on the ZnO clusters in the channel of HZSM-5; accordingly, the intensity of the purple luminescence band decreases dramatically as the ZnO loading exceeds 7.0 wt %.

It is noted that this purple luminescence band resulting from ZnO clusters has high quantum efficiency. As shown in Figure 13, where the LIL spectra of ZnO/HZSM-5 with 20.0 wt % ZnO loading excited at 325 and 244 nm are put together, we just see the purple band while the spectrum excited at 325 nm will be compressed into a straight line. For this sample, the intensity of the purple band is 674 times that of the orange band. And, for 7.0 wt % ZnO loading ZnO/HZSM-5, the intensity of the purple band is 13 times that for 20.0 wt % ZnO loading ZnO/HZSM-5. On the other hand, this may be the reason why the green band and orange band cannot be seen in Figure 12, in that case, 244 nm light is the excitation source.

As discussed above, there is a great amount of coordinatively unsaturated Zn sites, i.e., oxygen vacancies, in sub-nanometric ZnO clusters. Many studies[41−44] reported that oxygen vacancies are responsible for the green luminescence band from ZnO particles, and our previous works gave the same conclusion of this assignment. Similar to the nature of the green luminescence band from ZnO particles, this purple luminescence band centered at about 445 nm most likely originates from the coordinatively

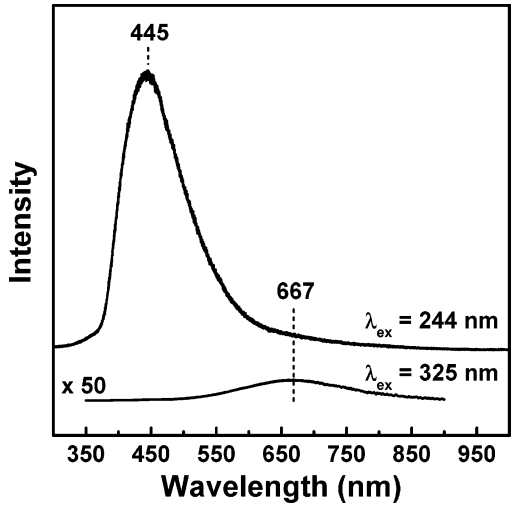

Figure 13. The intensity comparison between the LIL spectra of ZnO/HZSM-5 with 20.0 wt % ZnO loading, excited at 325 and 244 nm.

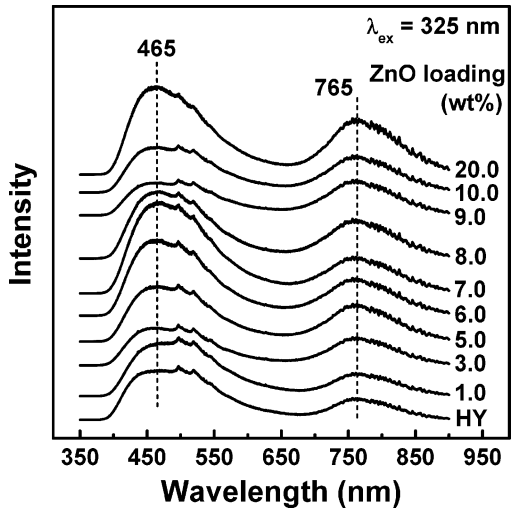

Figure 14. Laser-induced luminescence spectra of ZnO/HY with different ZnO loadings, excited at 325 nm.

unsaturated Zn sites in sub-nanometric ZnO clusters. Furthermore, the high density of these coordinatively unsaturated Zn sites in sub-nanometric ZnO clusters may be the reason for the high quantum efficiency of this purple band.

Figure 14 shows the LIL spectra of ZnO/HY with increasing ZnO loading, excited at 325 nm. There is not any luminescence signal related to ZnO for all these samples. This again suggests that no macrocrystalline ZnO exists for these ZnO/HY materials. Observed from the UV−visible absorption spectra of these samples, 325 nm light locates out of the absorption band of the ZnO clusters, meaning that this laser light cannot excite the electron of the ZnO clusters in ZnO/HY from the ground state to the upper electronic state. This is why no luminescence signal of ZnO clusters is exhibited in these ZnO/HY. The luminescence band centered at about 465 nm may be ascribed to the surface hydroxyl group on HY, and the luminescence band centered at about 765 nm possibly results from the amorphous alumina in HY, because this band also appears for Al_2O_3 samples.

Figure 15 shows the LIL spectra of ZnO/HY with increasing ZnO loading, excited at 244 nm. It is observed that, beside the luminescence band centered at 515 nm belongs to the host HY, a purple luminescence band with peak at 410 nm emerges and becomes stronger with increasing ZnO loading. As shown from

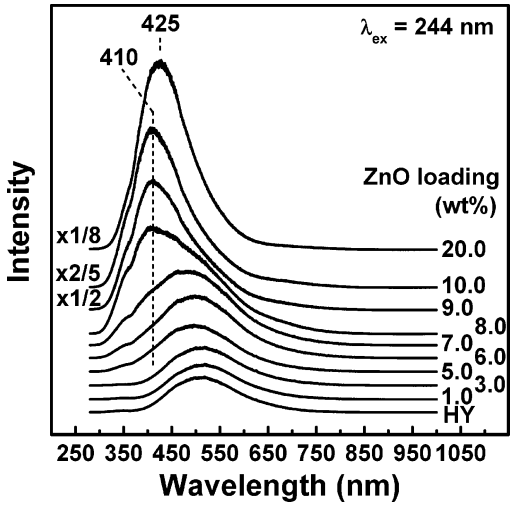

Figure 15. Laser-induced luminescence spectra of ZnO/HY with different ZnO loadings, excited at 244 nm.

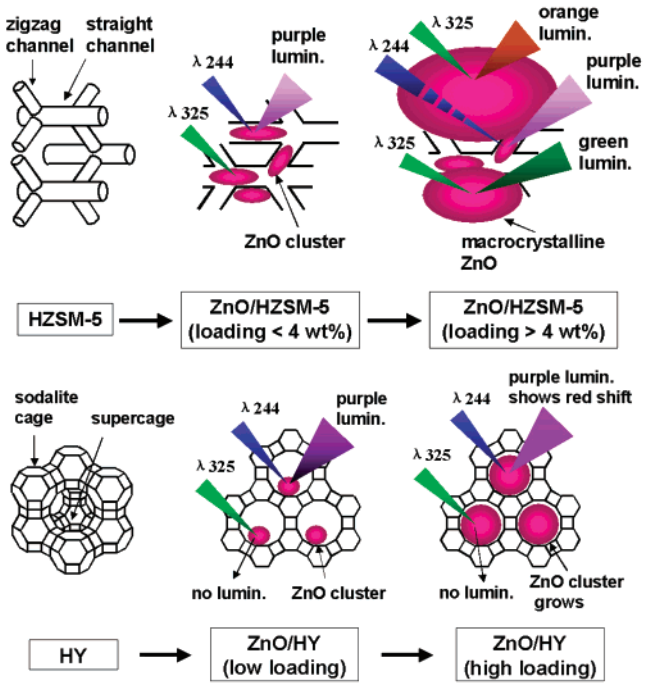

Figure 16. Schematic illustrations of ZnO clusters encapsulated in the pores of HZSM-5 and HY, and the luminescence behaviors of the ZnO species in these materials.

the UV−visible absorption spectra in Figure 2, these ZnO/HY samples exhibit that the absorbance at 244 nm wavelength increases drastically with increasing ZnO loading; this is agreeable with the intensity changing of the purple luminescence band of these samples excited by 244 nm light. These results again indicate that this purple luminescence band results from sub-nanometric ZnO clusters. When the ZnO loading is up to 20.0 wt %, the luminescence from the sample is glaringly strong. This means that this material has high quantum efficiency. On the other hand, the peak position of this purple band shifts from 410 to 425 nm for ZnO/HY with 20.0 wt % ZnO loading relative to that with 10.0 wt % ZnO loading; correspondingly, the absorption edge shown in Figure 2 obviously shows a red shift. It illustrates that this purple luminescence band from ZnO clusters possesses quantum size effect. Furthermore, the peak wavelength of the purple emission band from ZnO/HY is shorter than that from ZnO/HZSM-5, indicating that the ZnO clusters

in ZnO/HY are smaller than those in ZnO/HZSM-5. This is consistent with the conclusion from UV−visible absorption spectra.

The formation and the luminescence behaviors of sub-nanometric ZnO clusters in the pores of HZSM-5 and HY zeolites with increasing ZnO loading are illustrated schematically in Figure 16. The differences in the pore structure between these two zeolites cause the shape, size, quantity, and luminescent properties of ZnO clusters encapsulated in their pores to be different. For ZnO/HZSM-5, only a small amount of clubbed ZnO clusters, which exhibit a purple luminescence band centered between 432 and 445 nm, are prepared in the channels of HZSM-5 zeolite. But for ZnO/HY, a large amount of spherical ZnO clusters, which show a purple luminescence band centered between 410 and 425 nm, are confined in the supercages of HY zeolite.

Conclusions

By the incipient wetness impregnation method, sub-nanometric ZnO clusters can be introduced into the pores of microporous zeolite HZSM-5 (MFI type) and HY (FAU type), but the maximum amount of ZnO clusters that can be accommodated in these two zeolites are remarkably different. A large quantity of ZnO clusters can be accommodated in pores of zeolite HY, and no macrocrystalline ZnO exists. Physisorption values demonstrate that most ZnO clusers are located in the supercages of HY for the ZnO/HY samples. The absorption onset of the ZnO clusters, confined in the pores of microporous zeolite HZSM-5 and HY, appears below 265 nm. UV Raman spectra indicate that there are strong host−guest interactions between the framework oxygen atoms of zeolite and ZnO clusters. For ZnO/HY samples, the introduction of ZnO clusters into the supercages causes the changes of the Raman bands in the 900−1250 cm^{-1} region that are assigned to the Si−O stretching vibrations of HY. The existence of these interactions may be the reason why ZnO clusters are stabilized in the pores of zeolites. Laser-induced luminescence spectra show that the sub-nanometric ZnO clusters encapsulated in microporous zeolites exhibit a purple luminescence band centered at 410−445 nm, which possesses high quantum efficiency and quantum size effect. This purple luminescence band most likely originates from the coordinatively unsaturated Zn sites in the sub-nanometric ZnO clusters. On the other hand, the absorption edge and the purple luminescence band of ZnO clusters in the pores of HZSM-5 show a red shift in comparison with those of ZnO clusters in the pores of HY. This suggests that the shape and size of ZnO clusters formed in the pores are sensitive to the pore structure of zeolites.

Acknowledgment. This work was financially supported by the National Science Foundation of China (NSFC, grant 29927003 and grant 20273069) and the National Basic Research Program of China (grant 2003CB615806).

References and Notes

(1) Nakanishi, Y.; Miyake, A.; Kominami, H.; Aoki, T.; Hatanaka, Y.; Shimaoka, G. *Appl. Surf. Sci.* **1999**, *142*, 233.

(2) Huang, M.; Mao, S.; Feick, H.; Yan, H.; Wu, Y.; Kind, H.; Weber, E.; Russo, R.; Yang, P. *Science* **2001**, *292*, 1897.

(3) Birkmire, R. W. *Solar Energy Mater. Solar Cells* **2001**, *65*, 17.

(4) Reisfeld, R. *J. Alloys Compd.* **2002**, *341*, 56.

(5) Viswanatha, R.; Sapra, S.; Satpati, B.; Satyam, P. V.; Dev, B. N.; Sarma, D. D. *J. Mater. Chem.* **2004**, *14*, 661.

(6) Matsumoto, T.; Suzuki, J.; Ohnuma, M.; Kanemitsu, Y.; Masumoto, Y. *Phys. Rev. B* **2001**, *63*, 195322.

(7) Joswig, J. O.; Roy, S.; Sarkar, P.; Springborg, M. *Chem. Phys. Lett.* **2002**, *365*, 75.

(8) Khouchaf, L.; Tuilier, M. H.; Wark, M.; Soulard, M.; Kessler, H. *Microporous Mesoporous. Mater.* **1998**, *20*, 27.

(9) Readman, J. E.; Gameson, I.; Hriljac, J. A.; Edwards, P. P.; Anderson, P. A. *Chem. Commun.* **2000**, 595.

(10) Meneau, F.; Sankar, G.; Morgante, N.; Cristol, S.; Catlow, C. R. A.; Thomas, J. M.; Greaves, G. N. *Nucl. Instrum. Methods B* **2003**, *199*, 499.

(11) Zhang, W.; Shi, J.; Wang, L.; Yan, D. *Chem. Mater.* **2000**, *12*, 1408.

(12) Xia, H.; Tang, F. *J. Phys. Chem. B* **2003**, *107*, 9175.

(13) Zhao, X.; Lu, G.; Millar, G. J. *J. Porous Mater.* **1996**, *3*, 61.

(14) Türk, T.; Sabin, F.; Vogler, A. *Mater. Res. Bull.* **1992**, *27*, 1003.

(15) Anand, R.; Jyothi, T. M.; Rao, B. S. *Appl. Catal. A* **2001**, *208*, 203.

(16) Kazansky, V. B.; Borovkov, V. Yu.; Serykh, A. I.; van Santen, R. A.; Anderson, B. G. *Catal. Lett.* **2000**, *66*, 39.

(17) Li, C. *J. Catal.* **2003**, *216*, 203.

(18) Yu, J.; Li, M.; Liu, Z.; Feng, Z.; Xin, Q.; Li, C. *J. Phys. Chem. B* **2002**, *106*, 8937.

(19) Li, C.; Xiong, G.; Liu, J.; Ying, P.; Xin, Q.; Feng, Z. *J. Phys. Chem. B* **2001**, *105*, 2993.

(20) Xiong, G.; Yu, Y.; Feng, Z.; Xin, Q.; Xiao, F.; Li, C. *Microporous Mesoporous Mater.* **2001**, *42*, 317.

(21) Yu, Y.; Xiong, G.; Li, C.; Xiao, F. *Microporous Mesoporous Mater.* **2001**, *46*, 23.

(22) Wood, A.; Giersig, M.; Hilgendorff, M.; Vilas-Campos, A.; Liz-Marzan, L. M.; Mulvaney, P. *Austr. J. Chem.* **2003**, *56*, 1051.

(23) Haase, M.; Weller, H.; Henglein, A. *J. Phys. Chem.* **1988**, *92*, 482.

(24) Brus, L. E. *J. Chem. Phys.* **1984**, *80*, 4403.

(25) Brus, L. E. *J. Phys. Chem.* **1986**, *90*, 2555.

(26) Brunauer, S.; Deming, L. S.; Deming, E.; Teller, E. *J. Am. Chem. Soc.* **1940**, *62*, 1723.

(27) Li, J.; Xiong, G.; Feng, Z.; Liu, Z.; Xin, Q.; Li, C. *Microporous Mesoporous Mater.* **2000**, *39*, 257.

(28) Li, C.; Stair, P. C. *Catal. Today* **1997**, *33*, 353.

(29) Li, C.; Stair, P. C. *Stud. Surf. Sci. Catal.* **1997**, *105*, 599.

(30) Dutta, P. K.; Puri, M. *J. Phys. Chem.* **1987**, *91*, 4329.

(31) Scott, J. F. *Phys. Rev. B* **1970**, *2*, 1209.

(32) Dutta, P. K.; Twu, J. *J. Phys. Chem.* **1991**, *95*, 2498.

(33) Griffith, W. P. *J. Chem. Soc.* **1969**, *A9*, 1372.

(34) Dutta, P. K.; Rao, K. M.; Park, J. Y. *J. Phys. Chem.* **1991**, *95*, 6654.

(35) Knops-Gerrits, P. P.; Vos, D. E. D.; Feijen, E. J. P.; Jacobs, P. A. *Microporous Mater.* **1997**, *8*, 3.

(36) Dutta, P. K.; Shieh, D. C.; Puri, M. *J. Phys. Chem.* **1987**, *91*, 2332.

(37) Dutta, P. K.; Delbarco, B. *J. Phys. Chem.* **1988**, *92*, 354.

(38) Olson, D. H. *J. Phys. Chem.* **1970**, *74*, 2758.

(39) Zhai, Q.; Jiang, T.; Hu, W.; Guan, X.; Wang, W.; Qiu, S. *Mater. Res. Bull.* **2002**, *37*, 1837.

(40) Lü, X.; Xu, X.; Wang, N.; Zhang, Q.; Ehara, M.; Nakatsuji, H. *Chem. Phys. Lett.* **1998**, *291*, 445.

(41) Vanheusden, K.; Seager, C. H.; Warren, W. L.; Tallant, D. R.; Voigt, J. A. *Appl. Phys. Lett.* **1996**, *68*, 403.

(42) Vanheusden, K.; Warren, W. L.; Seager, C. H.; Tallant, D. R.; Voigt, J. A.; Gnade, B. E. *J. Appl. Phys.* **1996**, *79*, 7983.

(43) Studenikin, S. A.; Golego, N.; Cocivera, M. *J. Appl. Phys.* **1998**, *84*, 2287.

(44) van Dijken, A.; Meulenkamp, E. A.; Vanmaekelbergh, D.; Meijerink, A. *J. Phys. Chem. B* **2000**, *104*, 1715.